PERGAMON

Micron 31 (2000) 355–362

micron

www.elsevier.com/locate/micron

Valence state mapping of cobalt and manganese using near-edge fine structures

Z.L. Wang[a,*], J. Bentley[b], N.D. Evans[b]

[a]*School of Materials Science and Engineering, Georgia Institute of Technology, Atlanta, GA 30332-0245, USA*
[b]*Metals and Ceramics Division, Oak Ridge National Laboratory, Oak Ridge, TN 37831-6376, USA*

Abstract

The properties of transition metal oxides are related to the presence of elements with mixed valences. The spectroscopy analysis of the valence states is feasible experimentally, but a spatial mapping of valence states of transition metal elements is a challenge to existing microscopy techniques. In this paper, with the use of valence state information provided by the white lines and near-edge fine structures observed using the electron energy-loss spectroscopy (EELS) in a transmission electron microscope (TEM), a novel experimental approach is demonstrated to map the valence state distributions of Mn and Co using the ratio of white lines in the energy-filtered TEM. The valence state map is almost independent of specimen thickness in the thickness range adequate for quantitative EELS microanalysis. An optimum spatial resolution of ~2 nm has been achieved for a two-phase Co oxides.

Keywords: Electron energy-loss spectroscopy; Transmission electron microscope; Transition metal oxides

1. Introduction

Many properties of smart and functional materials are determined by the elements with mixed valences in the structure (Wang and Kang, 1998), by which we mean an element that has two or more different valences while forming a compound. In the perovskite structured $La_{1-x}A_xMnO_3$ (A = Ca, Sr, or Ba) colossal magnetoresistance (CMR) materials (Jin et al., 1994; Wang and Zhang, 1996), for example, the residual charges induced by a partial substitution of trivalent La^{3+} by divalent element A^{2+} are balanced by the conversion of Mn valence states between Mn^{3+} and Mn^{4+} (or Co^{3+} and Co^{4+} for Co) and the creation of oxygen vacancies as well, and the ionic structure of $La_{1-x}A_xMnO_{3-y}$ is

$$La^{3+}_{1-x}A^{2+}_{x}Mn^{3+}_{1-x+2y}Mn^{4+}_{x-2y}O^{2-}_{3-y}V^{O}_{y}$$

provided there is no residual charge trapped in the vacancy sites, where V^O_y stands for the fraction of oxygen vacancies. Valence transition between Mn^{3+} and Mn^{4+} is the key that leads to the transition from insulator to conductor and possibly the magnetoresistance.

Electron energy-loss spectroscopy (EELS) has been widely used in chemical microanalysis and the studies of solid state effects (Egerton, 1996). In EELS, the L ionization edges of transition-metal and rare-earth elements usually display sharp peaks at the near edge region which are known as *white lines*. For transition metals with unoccupied 3d states, the transition of an electron from 2p state to 3d levels leads to the formation of white lines. Numerous EELS experiments have shown that a change in valence state of cations introduces a dramatic change in the ratio of the white lines, leading to the possibility of identifying the occupation number of 3d orbital using EELS (Pease et al., 1986; Krivanek and Paterson, 1990; Kurata and Colliex, 1993; Pearson et al., 1993; Yuan et al., 1994; Yin and Wang, 1997; Wang et al. 1997a,b; Wang and Yin, 1998; Zhang et al., 1998). The spectroscopy analysis of the white line intensity is feasible for a region selected by the electron beam. In this paper, with the use of energy-filtered transmission electron microscopy (EF-TEM), a new experimental approach is introduced for mapping the distribution of a cation valences, allowing a direct identification of cations with different valence states. The valence state map is almost independent of the specimen thickness and it can be used to directly read out the local valence state from the image. A spatial resolution of ~2 nm has been demonstrated.

2. Experimental approach for mapping the valence states of Co and Mn

Fig. 1a shows an EELS spectrum of Co_3O_4. Several

* Corresponding author. Tel.: +404-894-8008; fax: +404-894-9140.
E-mail address: zhong.wang@mse.gatech.edu (Z.L. Wang).

0968–4328/00/$ - see front matter
PII: S0968-4328(99)00114-6

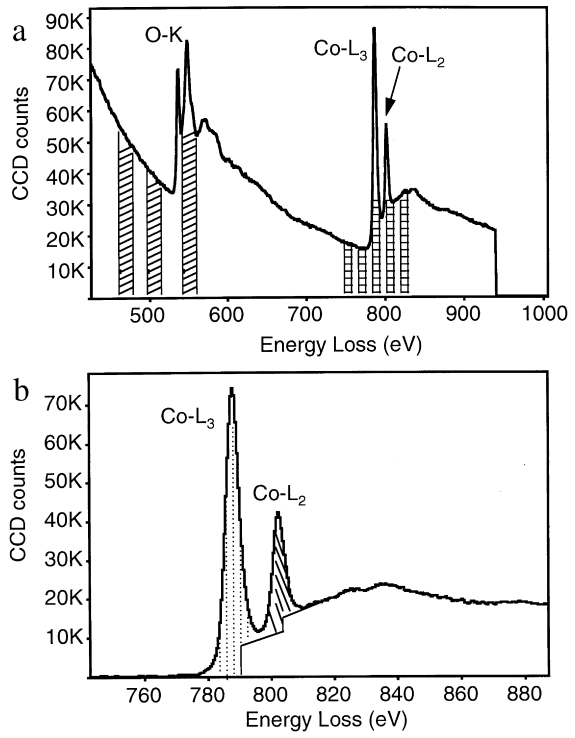

Fig. 1. (a) An EELS spectrum acquired from Co_3O_4, showing the five-window technique used to extract the intensities of the white lines and the three-window technique for O-K edge. (b) The Co-L edge after subtraction of the background, illustrating the background underneath the L_3 and L_2 lines.

techniques have been proposed to correlate the observed EELS signals with the valence states, the ratio of white lines the normalized white line intensity in reference to the continuous state intensity located ~50–100 eV beyond the energy of the L_2 line, and the absolute energy shift of the white lines. In this study, we use the white line intensity ratio that is calculated using a method demonstrated in Fig. 1b (Pearson et al., 1993). The background intensity was modeled by step functions in the threshold regions, as schematically shown in Fig. 1b. A straight line over a range of approximately 50 eV was fit to the background intensity immediately following the L_2 white line. This line was then modified into a double step of the same slope with onsets occurring at the white-line maxima. The ratio of the step heights is chosen to be 2:1 in accordance with the multiplicity of the initial states (four $2p_{3/2}$ electrons and two $2p_{1/2}$ electrons). Although there exist some disagreements in the literature about the calculation of the normalized white line intensity because the theory behind the white lines and their continuos background is rather complex (Thole and van der Laan, 1988), it appears, based on our experience, that this ratio of the white line intensities is likely to be a reliable and sensitive approach. This background subtraction procedure is followed consistently for all of the acquired spectra. The calculated L_3/L_2 is rather stable and is not sensitive to the specimen thickness.

EELS analysis of valence state is carried out in reference to the spectra acquired from standard specimens with known cation valence states. Since the intensity ratio of L_3/L_2 is directly related to the valence state of the corresponding element, a series of EELS spectra were acquired from several standard specimens with known valence states, an empirical plot of these data serves as the reference for determining the valence state of the element present in a new compound. The L_3/L_2 ratios of Co and Mn have been presented in our recent paper (Wang et al., 1999), which will be used as the standards in the analysis described below.

The information provided by EF-TEM is mostly about the elemental distribution in a thin section of a specimen (Reimer, 1995). To map the distribution of ionization states, an energy window of ~10 eV in width is required to isolate the L_3 from L_2 white lines. A five-window technique is introduced (see Fig. 1a): two images are acquired at the energy-losses prior to the L ionization edges, and they are to be used to subtract the background for the characteristic L edge signals; two images are acquired from the L_3 and L_2 white lines, respectively, and the fifth image is recorded using the electrons right after the L_2 line that will be used to subtract the continuous background underneath the L_3 and L_2 lines. To extract the L_3/L_2 image that is most sensitive to the valence state of Mn or Co, a background subtraction procedure illustrated in Fig. 1b needs to be carried out. This procedure can be easily done in the EELS spectrum, but for the energy-filtered image acquired in TEM under parallel illumination a different approach has to be taken, as given by

$$L_3/L_2 = \frac{I(L_3) - \alpha I(\text{post-lines})}{I(L_2) - \beta I(\text{post-lines})}, \quad (1)$$

where $I(L_3)$, $I(L_2)$ and I(post-lines) are the images recorded by positioning the energy selection window at the L_3, L_2 and the post L_2 line energy-losses, respectively, after subtracting the conventional background as ascribed by $A\exp(-r\Delta E)$; α and β are the adjustable parameters that represent the fractions of the continuous background below the L_3 and L_2 lines, respectively, as contributed by the single atomic scattering (as illustrated in Fig. 1b). The choices of the α and β factors may depend on the specimen thickness because the I(post-lines) image is strongly affected by the multiple scattering effect, while $I(L_3)$ and $I(L_2)$ are less affected. Eq. (1) represents the optimum choice for L_3/L_2 mapping in EF-TEM under the data collection conditions allowed by the Gatan Imaging Filter. A more accurate data treatment can be adopted in STEM.

To confirm the information provided by the L_3/L_2 images, the specimen composition is mapped from the integrated intensities of the O-K and Mn-$L_{2,3}$ ionization edges by following the routine procedure of EELS microanalysis (Egerton, 1996)

$$\frac{n_O}{n_{Mn}} = \frac{I_O(\Delta)}{I_{Mn}(\Delta)} \frac{\sigma_{Mn}(\Delta)}{\sigma_O(\Delta)}, \quad (2)$$

where $I_O(\Delta)$ and $I_{Mn}(\Delta)$ are the integrated intensities of the

O-K and Mn-L edges for an energy window Δ, respectively, above the ionization thresholds; $\sigma_{Mn}(\Delta)$ and $\sigma_O(\Delta)$ are the integrated ionization cross-sections for the corresponding energy window Δ, and they can be calculated by the SIGMAK2 and SIGMAL2 programs in the hydrogen-like atomic model. From the energy-filtered images, the distribution map of the atomic ratio O/Mn or O/Co can be calculated.

The EF-TEM experiments were performed using a Philips CM30 (300 kV) TEM, equipped with a Gatan image filtering (GIF) system. This TEM provides a high beam current needed for chemical imaging. The energy window width was selected to be 10 eV for Mn or 12 eV for Co, and it took 10–30 s (depending on specimen) exposure to acquire a single raw data image with satisfactory signal-to-noise ratio. The selection of the energy window width depends on the energy separation between the L_3 and L_2 lines. It took 2–4.5 min. to acquire a complete set of images. Specimen drift between different images was corrected after the acquisition, but it was important to ensure the least drift of the specimen during data acquisition.

3. Results

3.1. Mapping the valence states of Co using the white line ratio

The first specimen selected for illustrating the experimental approach is a directionally solidified eutectic ZrO_2/CoO (Bentley et al., 1993), which is composed of trilayer structures of ZrO_2, Co_3O_4 and CoO after heat treatment in a high oxygen partial pressure, with ideal geometry for studying CoO–Co_3O_4 interfaces. The differences in crystal structure, the coordination configuration of cations and the valence states result in dramatic differences in EELS spectra of CoO and Co_3O_4 (Bentley and Anderson, 1996). Shown in Fig. 2 is an one-dimensional spatially dispersed EELS spectra across a CoO–Co_3O_4 interface. The valence-loss spectra of the two phases are distinctly different. The O-K edge exhibits a double split peak for Co_3O_4 while no split for CoO. The white lines of the two structures are different not only in their relative intensity, but also in having a slight chemical shift ($\approx$ 1.5 eV). It was critical to select the width of the energy window and position it at the correct energies for acquired each group of data. The peak-to-peak energy between L_3 and L_2 is 15 eV and the full width of the line at 10% intensity cut-off is 7–8 eV, a choice of energy window width $\Delta = 12$ eV is adequately to separate the two lines as well as to ensure the signal-to-noise ratio.

Fig. 3 shows a group of energy-filtered image from a triple point in the CoO–Co_3O_4 specimen. The bright-field TEM image (Fig. 3a) shows one of the grains has a strong diffraction contrast. The energy-filtered images using the L_3 and L_2 lines (Fig. 3b and c) shows distinctly difference in contrast distribution due to a difference in the relative white line intensities (see Wang et al., 1999). The finally analyzed L_3/L_2 image clearly displays the distribution of cobalt oxides having different valence states (Fig. 3d), where the diffraction contrast disappears. The region with lower oxidation state (Co^{2+}) shows stronger contrast, and the ones with high oxidation states show darker contrast. Although the energy-filtered O-K edge image exhibits some diffraction contrast, the O/Co compositional ratio image greatly reduces the effect. The residual contrast seen in Fig. 3f might be due to the specimen drift during the 10 s exposure. The O/Co image was calculated from the images recorded from the O-K edge and the $L_3 + L_2$ white lines for an energy window width of $\Delta = 24$ eV. The high intensity region in the O/Co image indicates the relative high local concentration in oxygen (e.g. higher Co oxidation states), the low intensity region contains relatively less oxygen (e.g. lower Co valence state), entirely consistent with the information provided by the L_3/L_2 image.

Under the single scattering approximation, the intensities of the L_3 and L_2 lines scale up in proportional to the specimen thickness, thus, their ratio L_3/L_2 has little dependence on the specimen thickness. This result holds even for slightly thicker specimens because the near edge structure is less affected by the multiple plasmon scattering effect and the energies of the characteristic plasmon peaks are larger than the energy split between the L_3 and L_2 lines. Therefore, in the conventional thickness range for performing EELS microanalysis of $t/\Lambda < 0.8$, where t is the specimen thickness and Λ is the mean-free-path length of electron inelastic scattering, the L_3/L_2 image truly reflects the distribution of valence state across the specimen.

Fig. 4 shows another group of images recorded from the CoO–Co_3O_4 specimen. The L_3 and L_2 images display some contrast across the phases, while the image recorded from the post-line energy-loss region shows a small contrast variation (Fig. 4c) possibly because that the post-line region is dominated by the single atomic scatting properties and it is less affected by the solid state effects, provided the thickness-projected density of Co atoms is fairly uniform across the grains. The image from the O-K edge show some variation due to diffraction contrast as well as specimen thickness (Fig. 4d). In contrast, the L_3/L_2 image (Fig. 4e) and the O/Co image (Fig. 4f) show little dependence on the specimen thickness and the diffracting condition. This is uniquely suited for mapping the valence state distribution across the specimen.

To determine the optimum spatial resolution achieved in the L_3/L_2 image, a line scan across the CoO–Co_3O_4 interface at a 30 pixel average in width is displayed in Fig. 4g. The half width of the profile at the interface is about 2 pixels, which correspond to a resolution of $\sim$1.8 nm. The image across the interface in the O/Co image shows a half width of 3 pixels, which correspond to a resolution of $\sim$2.8 nm. It must be pointed out that a better resolution achieved in the L_3/L_2 image is likely due to the smaller width of the energy

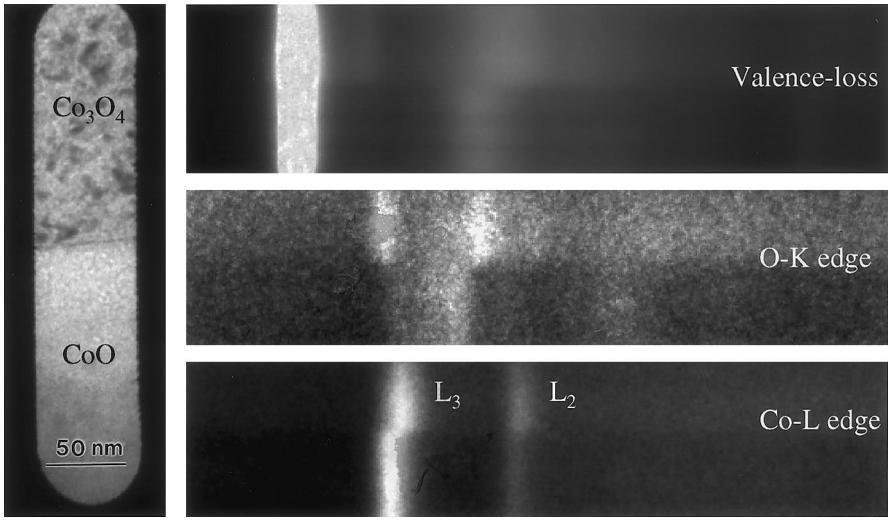

Fig. 2. Zero-loss bright-field TEM image of CoO–Co_3O_4 interface, showing the selection area aperture for forming the EELS spectra; spectrum lines for the low-loss region, the O-K edge, and the Co-L edge, exhibiting distinct differences in the intensities and energy positions of the characteristic peaks between CoO and Co_3O_4.

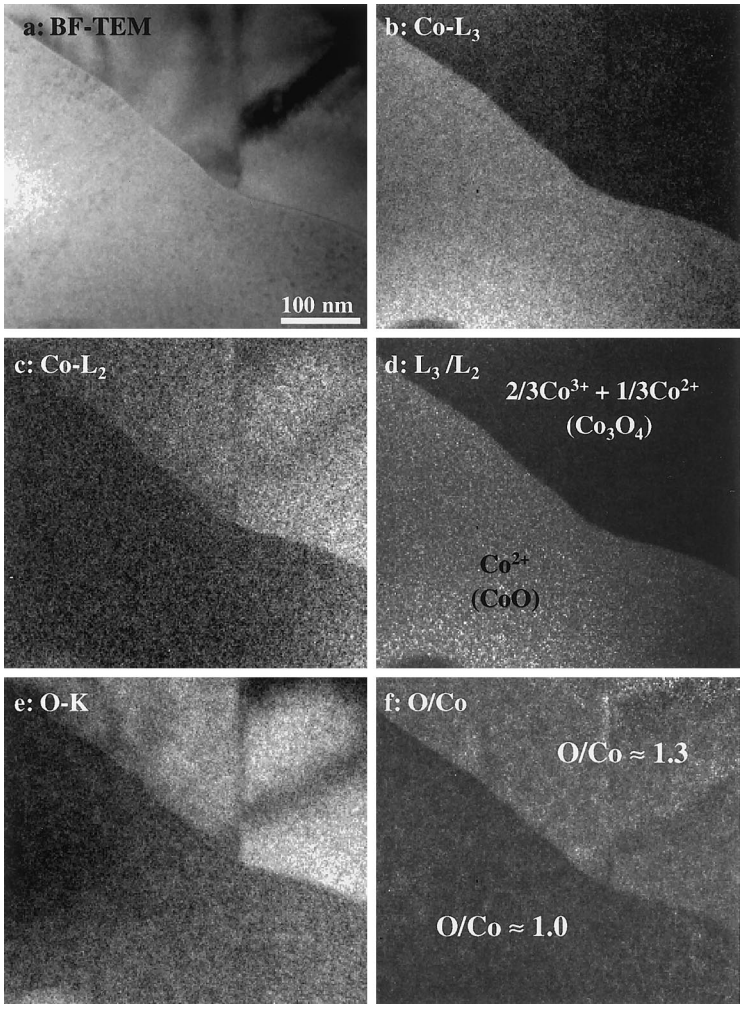

Fig. 3. A group of images recorded from the same specimen region using signals of (a) the zero-loss bright-field, (b) the Co-L_3 edge, (c) the Co-L_2 edge, (d) the L_3/L_2 ratio, (e) the O-K edge, and (f) the atomic concentration ratio of O/Co. The continuous background contributed from the single atom scattering has been removed from the displayed Co-L_3 and Co-L_2 images. The L_3/L_2 ratio image was calculated by taking $\alpha = 0.3$ and $\beta = 0.7$. The O/Co image is normalized in reference to the standard composition of CoO for the low portion of the image in order to eliminate the strong influence on the ionization cross-section from the white lines. Each raw image was acquired with an energy window width of $\Delta = 12$ eV except for O-K at $\Delta = 24$ eV.

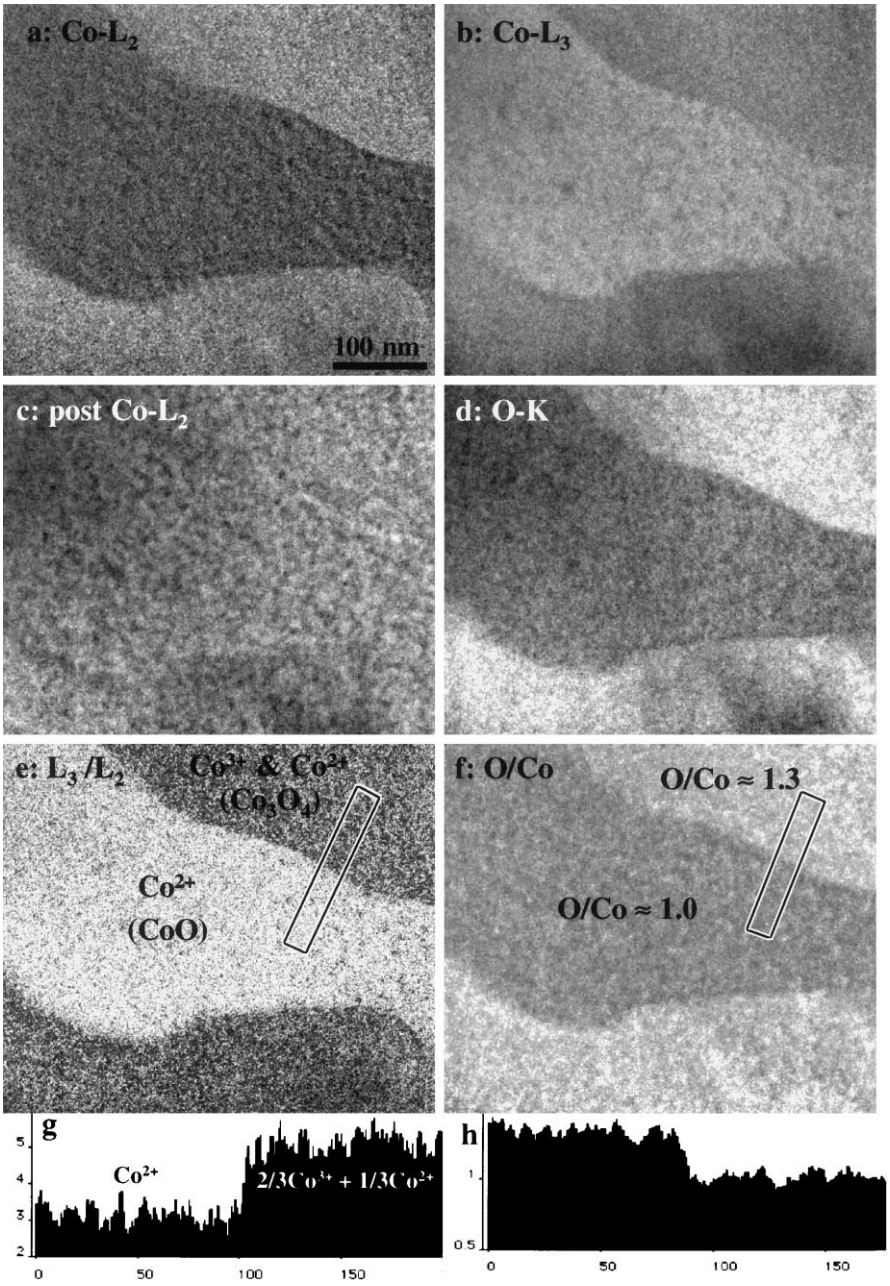

Fig. 4. A group of images recorded from the same specimen region using signals of: (a) the Co-L_2 edge; (b) the Co-L_3 edge; (c) the post Co-L_2 continuous energy-loss region; (d) the O-K edge; (e) the L_3/L_2 ratio; and (f) the atomic concentration ratio of O/Co. The continuous background contributed from the single atom scattering has been removed from the displayed Co-L_3 and Co-L_2 images. The L_3/L_2 ratio image was calculated by taking $\alpha = 0.3$ and $\beta = 0.8$. (g) A line scan across the CoO–Co_3O_4 interface in the L_3/L_2 image after making a 30 pixels of average in width parallel to the interface, showing the local average white line ratio. A comparison of the displayed numbers with the values measured from standard specimens (Wang et al., 1999), the regions corresponding to CoO and Co_3O_4 are apparent. (h) A line scan across the CoO–Co_3O_4 interface in the O/Co ratio image after making a 30 pixels of average in width parallel to the interface, from which the local compositions match very well to CoO and Co_3O_4. Each raw image was acquired with an energy window width of $\Delta = 12$ eV except for O-K at $\Delta = 24$ eV.

window ($\Delta = 12$ eV) than the $\Delta = 24$ eV used for O/Co image as well as the sharp shape of the white lines.

3.2. In situ observation of valence state transition of Mn

For demonstrating the application of the technique for a more complex case, a reduced MnO_x powder was prepared by in situ annealing (Wang et al., 1997a). A Gatan TEM specimen heating stage was employed to carry out the in situ EELS experiments, and the specimen temperature could be increased continuously from room temperature to 1000°C. The column pressure was kept at 3×10^{-8} Torr or lower during the in situ analysis. Due to the reduction of the oxide, multi-valences will be developed in the system. A

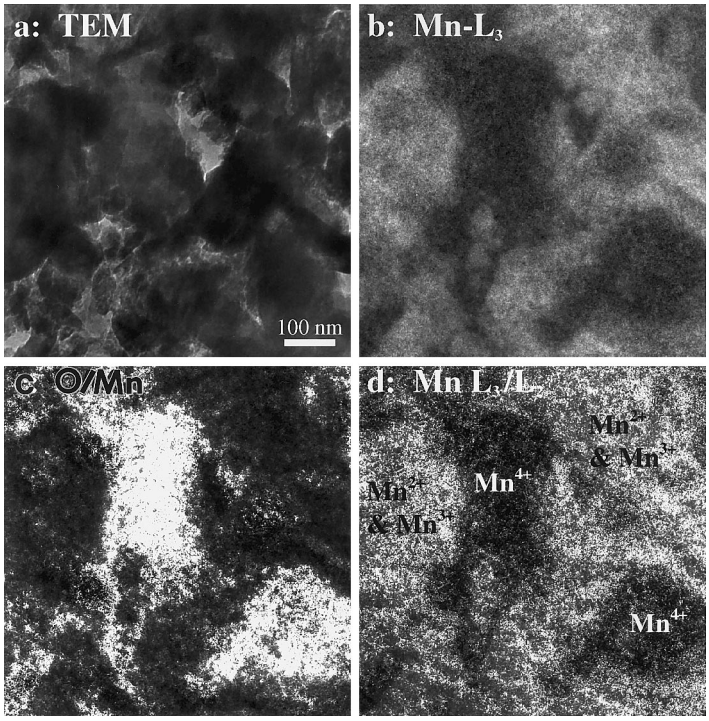

Fig. 5. A group of energy-filtered images acquired from the same specimen region of mixed phases of MnO_2 and Mn_3O_4: (a) The conventional bright-field TEM image; (b) the energy-filtered TEM images of Mn-L_3 white line; (c) the calculated Mn L_3/L_2 ratio image; and (d) the distribution of O/Mn in the region calculated according to Eq. (2) using the energy-filtered images from the O-K and Mn-L edges. The complimentary contrast of (c) to (d) proves the experimental feasibility of valence state mapping using the white line ratio. Each raw image was acquired with an energy window width of $\Delta = 10$ eV except for O-K at $\Delta = 20$ eV.

detailed analysis of this reduction process by EELS has been reported previously (Wang et al., 1997a, 1999). The results indicated that the reduction of MnO_2 occurs at 300°C. As the temperature reaches 450°C, the specimen is dominated by Mn^{2+} and Mn^{3+} and the composition is O/Mn = 1.3 ± 0.5, corresponding to Mn_3O_4.

To obtain a specimen with multi-valences, the in situ annealing of MnO_2 was carried out up to 350°C and then cool back to room temperature, and the resulting reduced phases were a mixture of oxides of Mn with valences of 2 + , 3 + and 4 + . This is a model system to be used for mapping the valence state distribution of Mn. Fig. 5 shows a group of images recorded from an agglomeration of MnO_x with different valences. The bright-field image hardly indicate any information about the valence states of Mn. The EF-TEM Mn-L_3 image reflects the distribution of Mn phases, but its contrast is approximately proportional to the local projected thickness of the specimen. The L_3/L_2 ratio image (Fig. 5c) directly gives the distribution of Mn^{4+}, Mn^{2+} and Mn^{3+}. The low intensity regions are Mn^{4+}, and the high intensity regions are the mixed valences of Mn^{2+} and Mn^{3+}, in correspondence to the formation of Mn_3O_4. To confirm this results, the atomic ratio O/Mn image is calculated from the images acquired from the O-K and Mn-L edges, and the result is given in Fig. 5d. The image clearly indicates that the regions with Mn^{4+} have higher O atomic concentration because of the balance of the cation charge. This is an excellent proof of the information provided by the L_3/L_2 image.

3.3. Phase separation using the near edge fine structure

The near-edge fine structure observed in EELS is closely related to the solid state effect and it is most sensitive to the bonding and near-neighbor coordination configurations. Phase and bonding mapping using the near-edge structure have been carried out for diamond (Batson et al., 1994; Mayer and Plitzko, 1996), in which the images were formed using the π^* and σ^* peaks in the C-K edge and the distribution of diamond bond was retrieved. The O-K edge displayed in Fig. 2 clearly shows the difference in the near edge structure of CoO from Co_3O_4. The first peak observed in the O-K of Co_3O_4 is separated by 12 eV from the main peak. Using an energy selection window of 6 eV in width it is possible to map the Co_3O_4 regions that generate this peak. Fig. 6b shows an energy-filtered TEM image from a region whose bright-field image is given in Fig. 6a. It is clear that the Co_3O_4 regions show stronger intensity, just as expected.

4. Discussion

There are several questions that need to be discussed relating to the L_3/L_2 image. The L_3/L_2 image has little dependence on either the specimen thickness or diffraction

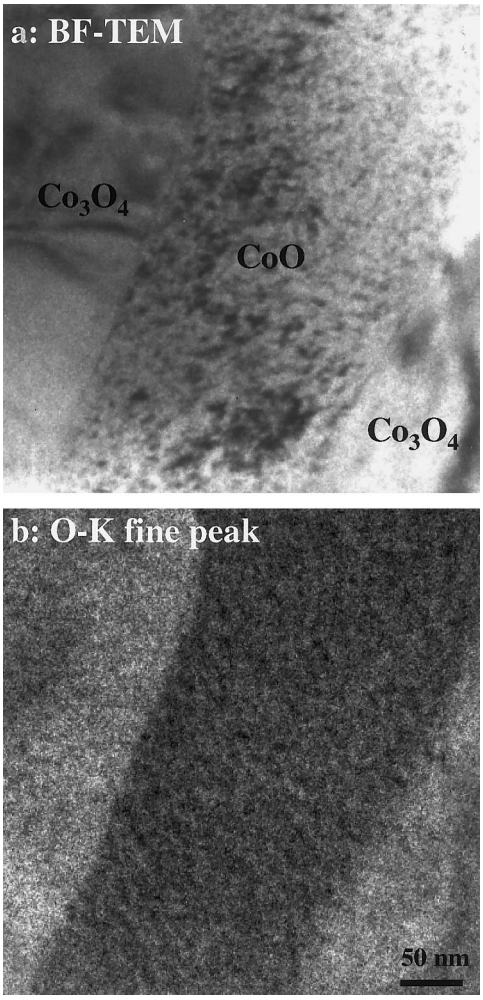

Fig. 6. (a) The bright-field TEM image and (b) the energy-filtered image recorded by selecting the sharp peak located at 532 eV in the O-K, displaying the distribution of the Co_3O_4 phase. Energy window width $\Delta = 6$ eV.

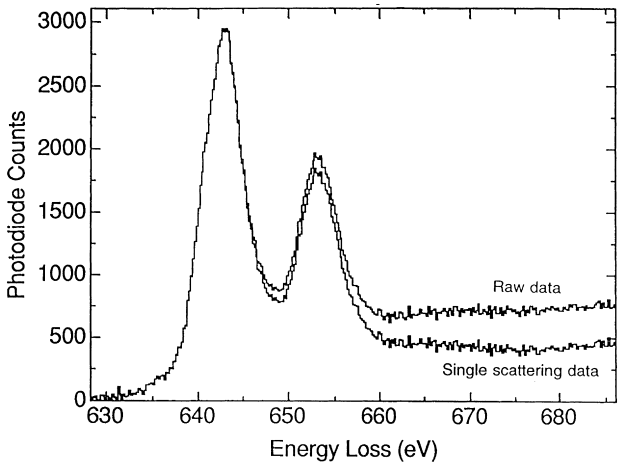

Fig. 7. A comparison of the Co-L edge before and after deconvoluting the low-loss spectrum, exhibiting the minor effect of multiple scattering on the intensities of white lines. The specimen thickness $t = 0.5\Lambda$.

effect in the thickness range adequate for EELS microanalysis ($t/\Lambda < 0.8$). For thicker specimens, the intensities of the L_2 line and the continuous post-line would be strongly affected by the specimen thickness. However, the L_3/L_2 ratio is much less sensitive to the specimen thickness, because the multiple scattering mainly affects the background underneath the L_3 and L_2 lines (see Fig. 7). Retrieving a single scattering profile would be possible by deconvolution if the entire spectra for each pixel were recorded. Unfortunately, the GIF system only captures the integrated data points and the deconvolution procedure cannot be carried out.

The calculation of the L_3/L_2 image is not critically sensitive to the selection of the α and β factors. This is possibly due to the flatter contrast of the post-line image, which depends mainly on the thickness-projected atom density and the diffraction effect. The best choices of the α and β factors would be to match the local average L_3/L_2 value with the standard data measured using spectroscopy in the region whose phase might be known. The choices of α and β should not result in large negative counts in the image due to over subtraction. One should avoid capture in a single image regions of large differences in thickness because the α and β factors might also depend on specimen thickness.

The subtraction of the continuous component beneath the white lines (see Fig. 1b) may not be trivial because its spectrum shape may be a broad peak rather than a smooth decay curve. One is advised to check the shape of the EELS spectra to ensure the procedure of data analysis.

The quality of the L_3/L_2 image is strongly affected by the quality of the L_2 image because of the dramatic magnification to the noise level. The critical challenge is the signal-to-noise ratio because of the finite beam current and the small energy window. A very thin region is inadequate for EF-TEM imaging because of the lack of the inelastic scattering signal, while a too thick region results in complexity in data quantification.

Finally, the O/Mn map displayed in this paper may not be the true atomic ratio in the specimen because the accuracy of EELS microanalysis strongly depends on the choice of the energy window. The most reasonable choice of energy window width is 50–100 eV in order to minimize the contribution from the near-edge fine structure (Colliex, 1985). In L_3/L_2 imaging, the width of the energy window is required to be no more than the energy split between the white lines, typically 10–15 eV. On the other hand, the heights of the L_3 and L_2 lines scale up in proportional to the local density of atoms. The O/Mn image can be used as a reliable reference for examining the information provided by the L_3/L_2 image.

5. Summary

For characterizing advanced materials that usually contain cations with mixed valences, EELS is a very powerful approach with a spatial resolution higher than any other spectroscopy techniques available. Based on the intensity

ratio of white lines, a new experimental approach has been demonstrated for mapping the valence states of Co and Mn in oxides using the energy-filtered transmission electron microscopy. The L_3/L_2 image has little dependence on either the specimen thickness or diffraction effects, and it is reliable for mapping the distribution of cation valences. An optimum spatial resolution of ~2.0 nm has been attained experimentally. This is a remarkable application of the EF-TEM for characterizing the electronic structure of magnetic oxides.

Acknowledgements

Research sponsored by the US NSF grant DMR-9733160, the Outstanding Oversea Young Scientist Award of China NSF (59825503), and by the Division of Materials Sciences, US Department of Energy, under contract DE-AC05-96OR22464 with Lockheed Martin Energy Research Corp., and through the SHaRE Program under contract DE-AC05-76OR00033 with Oak Ridge Associated Universities. Thanks to Drs A. Revcolevschi, S. McKernan and C.B. Carter for kindly providing the oxidized CoO specimen.

References

Batson, P.E., Browning, N.D., Muller, D.A., 1994. EELS at Buried Interfaces: Pushing Towards Atomic Resolution, MSA Bulletin, 24. Microscopy Society of America, pp. 371–374.

Bentley, J., Anderson, I.M., 1996. Spectrum Lines Across Interfaces by Energy-Filtered TEM. In: Bailey, G.W., Corbett, J.M., Dimlich, R.V.W., Michael, J.R., Zaluzec, N.J. (Eds.). Proc. Microscopy and Microanalysis, San Francisco Press, San Francisco, pp. 532–533.

Bentley, J., McKernan, S., Carter, C.B., Revcolevschi, A., 1993. Microanalysis of Directionally Solidified Cobalt Oxide-Zirconia Eutectic. In: Armstrong, J.T., Porter, J.R. (Eds.). Microbeam Analysis, 2. pp. S286–287 suppl.

Botton, G.A., Appel, C.C., Horsewell, A., Stobbs, W.M., 1995. Quantification of the EELS near-edge structures to study Mn doping in oxides. J. Microsc. 180, 211–216.

Colliex, C., 1985. An illustrative view on various factors governing the high spatial resolution capabilities in EELS microanalysis. Ultramicroscopy 18, 131–150.

Egerton, R.F., 1996. Electron Energy-Loss Spectroscopy in the Electron Microscope, 2. Plenum Press, New York.

Jin, S., Tiefel, T.H., McCormack, M., Fastnacht, R.A., Ramech, R., Chen, L.H., 1994. Thousandfold change in resistivity in magnetoresistive La–Ca–Mn–O films. Science 264, 413–415.

Krivanek, O.L., Paterson, J.H., 1990. ELNES of 3d transition-metal oxides: I. Variations across the periodic table. Ultramicroscopy 32, 313–318.

Kurata, H., Colliex, C., 1993. Electron-energy loss core-edge structures in manganese oxides. Phys. Rev. B 48, 2102–2108.

Mayer, J., Plitzko, J.M., 1996. Mapping of ELNES on a nanometre scale by electron spectroscopic imaging. J. Microsc. 183, 2–8.

Pearson, D.H., Ahn, C.C., Fultz, B., 1993. White lines and d-electron occupancies for the 3d and 4d transition metals. Phys. Rev. B 47, 8471–8478.

Pease, D.M., Bader, S.D., Brodsky, M.B., Budnick, J.I., Morrison, T.I., Zaluzec, N.J., 1986. Anomalous L_3/L_2 white line ratios and spin pairing in 3d transition metals and alloys: Cr metals and $Cr_{20}Au_{80}$. Phys. Lett. 114A, 491–494.

Reimer, L. (Ed.), 1995. Energy-Filtering Transmission Electron Microscopy Springer Series in Optical Sciences, 71. Springer, Berlin.

Thole, B.T., van der Laan, G., 1988. Branching ratio in X-ray absorption spectroscopy. Phys. Rev. B 38, 3158–3169.

Wang, Z.L., Kang, Z.C., 1998. Functional and Smart Materials—Structural Evolution and Structure Analysis, Plenum Press, New York.

Wang, Z.L., Zhang, J., 1996. Tetragonal domain structure magnetoresistance of $La_{1-x}Sr_xCoO_3$. Phys. Rev. B 54, 1153–1158.

Wang, Z.L., Yin, J.S., 1998. Cobalt valence and crystal structure of $La_{0.5}Sr_{0.5}CoO_{2.25}$. Philos. Mag. B 77, 49–65.

Wang, Z.L., Yin, J.S., Zhang, J.Z., Mo, W.D., 1997a. In-situ analysis of valence conversion in transition metal oxides using electron energy-loss spectroscopy. J. Phys. Chem. B 101, 6793–6798.

Wang, Z.L., Yin, J.S., Jiang, Y.D., Zhang, J., 1997b. Studies of Mn valence conversion and oxygen vacancies in $La_{1-x}Ca_xMnO_{3-y}$ using electron energy-loss spectroscopy. Appl. Phys. Lett. 70, 3362–3364.

Wang, Z.L., Yin, J.S., Jiang, Y.D., 1999. EELS analysis of cation valence states and oxygen vacancies in magnetic oxides. Micron, in press.

Yin, J.S., Wang, Z.L., 1997. Ordered self-assembling of tetrahedral oxide nanocrystals. Phys. Rev. Lett. 79, 2570–2573.

Yuan, J., Gu, E., Gester, M., Bland, J.A.C., Brown, L.M., 1994. Electron energy-loss spectroscopy of Fe thin-films on GaAs(001). J. Appl. Phys. 75, 6501–6503.

Zhang, Z.J., Wang, Z.L., Chakoumakos, B.C., Yin, J.S., 1998. Temperature dependence of cation distribution and oxidation state in magnetic Mn–Fe ferrite nanocrystals. J. Am. Chem. Soc. 120, 1800–1804.